Insights into the origin of coexisting A$_1$- and A$_2$-type granites: Implications from zircon Hf-O isotopes of the Huayuangong intrusion in the Lower Yangtze River Belt, eastern China

Xiao-Yan Jiang [a,*], Ming-Xing Ling [c,e], Kai Wu [a,f], Zhe-Kun Zhang [a,f], Wei-Dong Sun [b,d,e,f,**], Qing-Lin Sui [g], Xiao-Ping Xia [c]

[a] CAS Key Laboratory of Mineralogy and Metallogeny, Guangzhou Institute of Geochemistry, Chinese Academy of Sciences, Guangzhou 510640, China
[b] Laboratory for Marine Mineral Resources, Qingdao National Laboratory for Marine Science and Technology, Qingdao 266237, China
[c] State Key Laboratory of Isotope Geochemistry, Guangzhou Institute of Geochemistry, Chinese Academy of Sciences, Guangzhou 510640, China
[d] Center of Deep Sea Research, Institute of Oceanology, Chinese Academy of Sciences, Qingdao 266071, China
[e] CAS Center for Excellence in Tibetan Plateau Earth Sciences, Chinese Academy of Science, Beijing 100101, China
[f] University of Chinese Academy of Sciences, Beijing 100094, China
[g] Xi'an Institute of Geology and Mineral Resources, Xi'an, Shanxi 710054, China

ARTICLE INFO

ABSTRACT

The origin of A-type granites has been the subject of great debate, especially the enigmatic synchronous A$_1$- and A$_2$-type granites. Cretaceous (~125 Ma) A$_1$- and A$_2$-type granites are common throughout the Lower Yangtze River Belt (LYRB), eastern China. However, their genesis still remains unclear. In this study, in-situ zircon O isotopic data and chemical compositions of the Huayuangong (HYG) A-type granites in Anhui province, provide new insights into the origin and evolution of A-type granites in the LYRB, as well as the genetic link for synchronous A$_1$- and A$_2$-type granites. The HYG granites include syenogranite (75.9 wt%–76.6 wt% SiO$_2$) and quartz syenite (66.1 wt%–66.9 wt% SiO$_2$). Both are metaluminous and belong to ferroan series. They are characterized by high alkalis (K$_2$O + Na$_2$O = 8.36 wt%–8.55 wt% and 11.7 wt%–11.9 wt%), high field strength elements (Zr + Nb + Ce + Y = 909 ppm–1269 ppm and 1092 ppm–1329 ppm) and high Ga/Al ratios (10,000 * Ga/Al = 4.91–4.96 and 2.64–2.68). The zircon saturation thermometer results indicate high magmatic temperatures (896–964 °C and 860–882 °C). All those geochemical features show an A-type granite affinity. They can be further classified into A$_1$- and A$_2$-type granites, corresponding to reduced and oxidized A-type granites, respectively. Additionally, the in-situ zircon O-Hf isotope compositions are also distinctly different, with $\delta^{18}O$ = 4.7‰–6.0‰ and $\epsilon_{Hf}(t)$ = −1.5 to −3.6 for A$_1$-type granites, and $\delta^{18}O$ = 7.0‰–7.8‰ and $\epsilon_{Hf}(t)$ = −3.3 to −6.9 for A$_2$-type granites. The geochemical signatures and newly discovered $\delta^{18}O$ and $\epsilon_{Hf}(t)$ values of the two A-type granite subgroups, indicate that they were derived from different source components and under disparate physicochemical conditions (e.g., temperature, redox state and water contents). Lithospheric mantle-like isotopic data from zircons of A$_1$-type granites suggest fractional crystallization of reduced, anhydrous basaltic magmas resulting in the formation of A$_1$-type granites. In contrast, A$_2$-type granites with relatively high $\delta^{18}O$ and negative εHf values were generated from partial melting of the lithospheric mantle which was metasomatized by slab-derived melts/fluids. The coexisting A$_1$- and A$_2$-type granites were formed under the extensional setting where lithospheric thinning and asthenosphere upwelling occurred.

© 2018 Elsevier B.V. All rights reserved.

1. Introduction

Granitoids are the most abundant constituents of the upper continental crust and closely related to the tectonic evolution. However, the source and evolutionary trends of granites are still hot debated. For example, are they produced by fractional crystallization of mantle-derived basaltic melts or reworking of preexisting crustal materials? A-type granites constitute a distinct group of granitoid rocks, with high alkali contents, high field strength element (HFSE) concentrations, Ga/Al ratios, as well as high magmatic temperatures (Bonin, 2007; Collins et al., 1982; Landenberger and Collins, 1996; Loiselle and Wones, 1979; Patiño Douce, 1997). Additionally, they commonly evolve and/or crystallize in shallow magma chambers and are emplaced in

* Corresponding author.
** Correspondence to: W.D. Sun, Laboratory for Marine Mineral Resources, Qingdao National Laboratory for Marine Science and Technology, Qingdao 266237, China.
E-mail addresses: jiangxy@gig.ac.cn (X.-Y. Jiang), weidongsun@qdio.ac.cn (W.-D. Sun).

extensional tectonic settings (Bonin, 2007; Eby, 1990; Eby, 1992; Patiño Douce, 1997). Different classification schemes have been proposed to describe and explain their petrogenesis and geological significance (Dall'Agnol and Oliveira, 2007; Eby, 1992; King et al., 1997; Whalen et al., 1987). The earliest and most common one divided A-type granites into A_1 and A_2 subgroups (Eby, 1992). A-type granites are also classified into aluminous and alkaline subgroups (King et al., 1997). A-type granites are generally considered to have crystallized under conditions of low water-content and low f_{O2} (e.g.,Bonin, 2007; Patiño Douce, 1997). However, some studies also suggest that A-type granites could be derived from melts with appreciable water contents under oxidizing conditions (Dall'Agnol et al., 1999; Dall'Agnol et al., 2005; Dall'Agnol and Oliveira, 2007). Recent studies found some A-type granite plutons containing both A_1 and A_2 subgroups, the genesis of which is poorly constrained. Varying degrees of fractional crystallization (Rajesh, 2000), mantle metasomatism (Li et al., 2012) or distinct source components (Kemp et al., 2005) are thought to be involved. Therefore, the mechanism that controls the formation of A-type granites still needs in-depth study.

Oxygen isotope analysis is effective in tracing the involvement of crustal/mantle materials in the magmatic source and providing robust constraints on hydrothermal processes during the magmatic evolution (Eiler, 2001; Bindeman et al., 2005; Bindeman and Serebryakov, 2011; Bindeman and Valley, 2001; Spencer et al., 2017). Magmatic zircon is recognized as the premier geochemical tracer of primary oxygen isotopic composition (Valley, 2003). The mantle is a remarkably homogeneous oxygen isotope reservoir (Eiler, 2001), and igneous zircons in equilibrium with pristine mantle-derived magmas have a narrow range of $\delta^{18}O = 5.3 \pm 0.3‰$ (1SD, Cavosie et al., 2009; Valley et al., 1998). Zircon oxygen values ($\delta^{18}O$) are insensitive to fractional crystallization because the fractionation $\Delta^{18}O$ (WR-Zrc) increases at nearly the same rate as $\delta^{18}O$ (WR) (Valley, 2003). Therefore, significant higher $\delta^{18}O$ than the mantle value fingerprints the intra-crustalcomponents recycling, such as either sedimentary rocks (10 to 30‰) or altered volcanic rocks (to 20‰) (Eiler, 2001; Valley, 2003; Kemp et al., 2007; Spencer et al., 2017). Low-$\delta^{18}O$ (<4.6–4.7‰ at 95% confidence level) igneous rocks require a certain amount of seawater ($\delta^{18}O = 0‰$) or meteoric water ($\delta^{18}O < 0‰$) involvement at relatively high temperatures (e.g.,Bindeman and Serebryakov, 2011; Bindeman and Valley, 2001).

Large-scale late Mesozoic magmatic activities occurred in the Lower Yangtze River belt (LYRB), are closely related to the Cu, Au, Fe, Pb, Zn and Ag mineralizations (Li et al., 2013a; Ling et al., 2009; Sun et al., 2003; Sun et al., 2007; Wang et al., 2013). Cretaceous A-type granites are part of this magmatic activity and are distributed along the LYRB (Li et al., 2012; Xing and Xu, 1994). Both A_1- and A_2-type granites were emplaced during the same period at 125 ± 5 Ma (Gu et al., 2017; Li et al., 2011; Li et al., 2012; Wang et al., 2018; Yan et al., 2015). Previous studies on A-type granites are mainly aimed at the age distribution, whole-rock geochemical characteristics, and tectonic settings (Gu et al., 2017; Li et al., 2011; Li et al., 2012; Wang et al., 2018; Xing and Xu, 1994). The source components and magmatic evolution of A-type granites are debatable, and the contribution of the mantle is still unclear (e.g.,Gu et al., 2017; Jiang et al., 2018; Li et al., 2011; Li et al., 2012; Wang et al., 2018; Xing and Xu, 1994). Particularly, little attention has been paid to the petrogenesis and evolution processes of coexisting A_1- and A_2-type granites.

In this contribution, we focus on the HYGA-type granite in the LYRB, which is special because of the coexisting A_1- and A_2-subgroups. We present in-situ zircon O-Hf isotope compositions, whole-rock major and trace elements for the A-type granite. These results are used to shed new light on the characteristics of the A-type granites, determine the petrogenesis of the coexisting A_1- and A_2-type granites, and constrain the tectonic environment for the late Mesozoic A-type granites in the LYRB.

2. Geological background

The LYRB is located on the northeastern margin of the Yangtze Block (Fig.1), adjacent to the Dabie-Sulu orogenic belt, and separated from the Cathaysia Block by the Jiangshan-Shaoxing fault in the south (Fig.1). The Neoproterozoic low-grade clastic metasedimentary series with minor volcanic rocks and Paleozoic-Triassic sedimentary strata were subsequently intruded by Late Mesozoic magmatic rocks (150 to 110 Ma) (Fig.1; Yang and Zhang, 2012). Previous chronology data suggest that igneous rocks could be divided into three separate stages, ca. 150 Ma to 136 Ma, ca. 136 to 130 Ma, and ca. 130 Ma and 120 Ma. They are corresponding to adakitic rocks (e.g.,Wu et al., 2012; Yang and Zhang, 2012), subvolcanic rocks (diorite porphyry, granite porphyry and their volcanic counterparts) (e.g.,Chen et al., 2014; Wu et al., 2012; Xie et al., 2011; Zhang et al., 2009), and A-type granitoids and bimodal volcanic rocks (Gu et al., 2017; Li et al., 2011; Li et al., 2012; Ling et al., 2009; Xie et al., 2011; Xing and Xu, 1994), respectively.

The HYG pluton is located in the Anqing-Guichi area (Figs. 1 and 2) and intrudes into the Late Neoproterozoic metasedimentary and metavolcanic rocks and Paleozoic marine clastic sediments and carbonates (Li et al., 2012; Wang et al., 2018). Previous zircon U-Pb studies ofthe HYG syenogranite and quartz syenite yield weighted mean $^{206}Pb/^{238}U$ ages of 125 ± 1 Ma to 127 ± 2 Ma and 124 ± 1 Ma to 127 ± 3 Ma, respectively (Li et al., 2012; Wang et al., 2018), suggesting emplacement of the syenogranite and quartz syenite at ca. 125 Ma. The HYG syenogranites are dominated by perthitic K-feldspar (60–70 vol %), with less common quartz (20–25 vol%), plagioclase (~5 vol%) and minor interstitial biotite (Fig.2). Plagioclase is commonly zoned, displaying polysynthetic twins, and K-feldspar generally exhibit microcline twinning. The subhedral to euhedral biotites display a foxy red brown color and locally occur as mineral aggregates. Accessory minerals include zircon, magnetite and titanite. Quartz syenite consists of plagioclase (~5 vol%), K-feldspar (65–75 vol%), quartz (5–10 vol%), biotite $\pm$ amphibole (~5 vol%), with accessory apatite, titanite, magnetite and zircon (Fig.2). Plagioclase is oscillatory zoned and K-feldspar shows microcline twinning.

3. Analytical methods

3.1. Whole-rock major and trace elements analysis

Fresh rock samples were processed to finer than 200 mesh particle size. The major element analyses were conducted by the ALS Laboratory Group, Analytical chemistry and testing services. A representative aliquot of the sample powder was dried at 105 °C for 4 h and treated to produce glass beads that were analyzed using an X-ray fluorescence spectrometer. Relative standard derivation for major-element contents was <5%.

Trace element analyses of whole rock were measured on Agilent 7700e ICP-MS at the Wuhan Sample Solution Analytical Technology Co., Ltd., Wuhan, China. The detailed sample-digesting procedure and analytical precision and accuracy were identical to those of Liu et al. (2008). An internal standard Rh solution was used to monitor the signal drift of the spectrometer during analysis. Standards materials AGV-2, BHVO-2, BCR-2 and RGM-2 were chosen for correcting element concentrations. The precision during trace element analysis was generally better than 5%.

Bulk F concentrations of seven rock samples were determined using an alkaline fusion method to extract F at ALS Laboratory Group, Analytical chemistry and testing services. The 200 mesh powered samples were mixed with KOH and MgO at a mass ratio of 1:3:1, and then fused in anelectric furnace at 900 °C for 30 to 40 min. The fused samples were dissolved by deionized water to form solutions for measurement. Fluorine was analyzed using F-ELE81a Ion Selective Electrode (ISE). The detection limit is around 20 ppm.
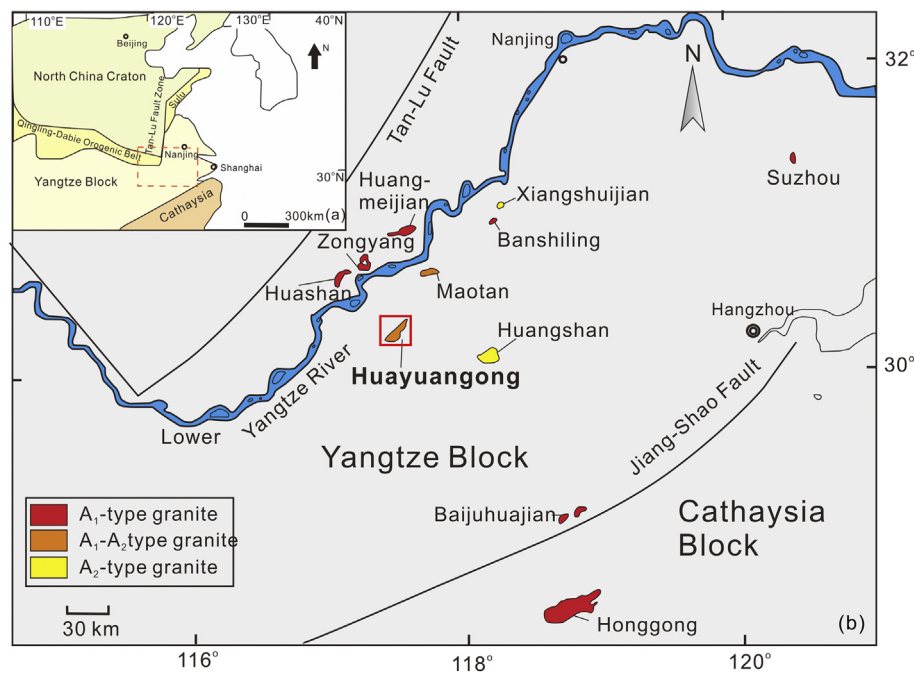
Major and trace elements are listed in Table1.

Fig.1. Geological map of the Lower Yangtze River Belt (LYRB): (a)tectonic sketch map of eastern China; (b)distribution of the Late Mesozoic A-type granitic rocks in the Lower Yangtze River Belt (after Li et al., 2012).

3.2. In-situ zircon O isotope analysis

Zircon grains were separated from representative rock samples using standard heavy liquid and magnetic techniques, and then hand-picked under a binocular microscope. Single crystal grains were mounted by use of epoxy resin and polished to expose the central surface. Transmitted and reflected light micrographs as well as cathodoluminescence (CL) images (Fig.3) were collected to reveal their internal structures. Prior to SIMS analysis, the mount was vacuum-coated with high-purity gold.

Zircon oxygen isotopes were conducted on Cameca 1280HR SIMS at Guangzhou Institute of Geochemistry, Chinese Academy of Sciences (GIG-CAS). The analysis spot size 20 μm was applied to the analysis. Oxygen isotopes were measured by Cs^+ ion source, in multi-collector mode with two off-axis Faraday cups. Detailed analytical procedures are the same as those described by Li et al. (2010a). Zircon standard Penglai ($\delta^{18}O = 5.31‰$) was used to correct the instrumental mass fractionation factor (IMF) (Li et al., 2010b). The internal precision of a single analysis was generally better than 0.20‰ (1σ standard error) for $^{18}O/^{16}O$ ratio. During the sections of this study, the external precision was constrained by the reproducibility of repeated analyses of Penglai standard, which was 0.34‰ (2SD, n = 17). An in-house zircon standard Qinghu was also measured as an unknown interspersed with other unknowns. Measurements of Qinghu zircon yield a weighted mean of $\delta^{18}O$ = 5.62 ± 0.48‰ (2SD, n = 6), consistent within errors with the reported value of 5.4 ± 0.2‰ (Li et al., 2013b). Zircon O-isotope data are listed in Table2.

3.3. Zircon Lu-Hf isotope analysis

Lu-Hf isotopic analyses were conducted on the same zircon grains which were previously measured O isotopic compositions. In-situ zircon Lu-Hf isotopic measurements were performed on a Neptune Plus MC-ICP-MS, coupled with a RESOlution 193 nm laser ablation system at the GIG-CAS. The laser beam diameter is 45 μm with the repetition rate 6 Hz and energy density ~4 J cm^{-2}. The detailed description of

analytical procedures and calibration methods can be found in Wu et al. (2006). Plešovice was analyzed during the section to evaluate the reliability of unknown samples measurement. The mass bias of $^{176}Hf/^{177}Hf$ was normalized to $^{179}Hf/^{177}Hf = 0.7325$ with an exponential law. Zircon standard Plešovice yielded a weighted average $^{176}Hf/^{177}Hf$ ratio of 0.282490 ± 0.000025 (2SD, N = 24), which is consistent with the reported value (0.282482 ± 0.000013 (2SD)) (Sláma et al., 2008) within errors. In-situ zircon Lu-Hf isotope ratios and $\varepsilon_{Hf}(t)$ values are presented in Table2.

3.4. Whole-rock Nd isotope analysis

For Nd isotopic analyses, ~100 mg of sample material was dissolved in HF + HNO$_3$ acid in Teflon bombs at ~195 °C for two days. Strontium and rare earth elements (REE) were separated using cation columns; Nd fractions were further separated in HDEHP-coated Kef columns. Neodymium isotopic analyses were conducted using a Micromass Isoprobe multi-collector–ICP-MS (MC–ICP-MS) at the State Key Laboratory of Isotope Geochemistry, GIGCAS. Analytical procedures were similar to those described by Li et al. (2004). The MC–ICP-MS was operated in static mode and analyses of the Shin Etsu JNdi-1 standard yielded $^{143}Nd/^{144}Nd$ values of 0.512117 ± 9 (2σ, n = 5). To correct for mass fractionation, measured Nd isotope ratios were normalized toa composition of $^{146}Nd/^{144}Nd = 0.7219$. Analyses of the Shin Etsu JNdi-1standards yielded $^{143}Nd/^{144}Nd$ ratios that were within error of the recommended values of $^{143}Nd/^{144}Nd = 0.512115$, respectively (Tanaka et al., 2000). Isotopic compositions and calculated $\varepsilon_{Nd}(t)$values are listed in Appendix Table1.

3.5. Apatite major and trace elements analysis

Apatite crystals were separated and then mounted in an epoxy grain mount. The mount was then polished to expose a cross section of the apatite grains for electron microprobe (EMP) and LA-ICP-MS analyses.

Major elements in the apatite were analyzed using a JXA8230 JEOL electron microprobe operated with wavelength-dispersive spectrometers (WDS) at the Shandong Bureau of China Metallurgical Geology
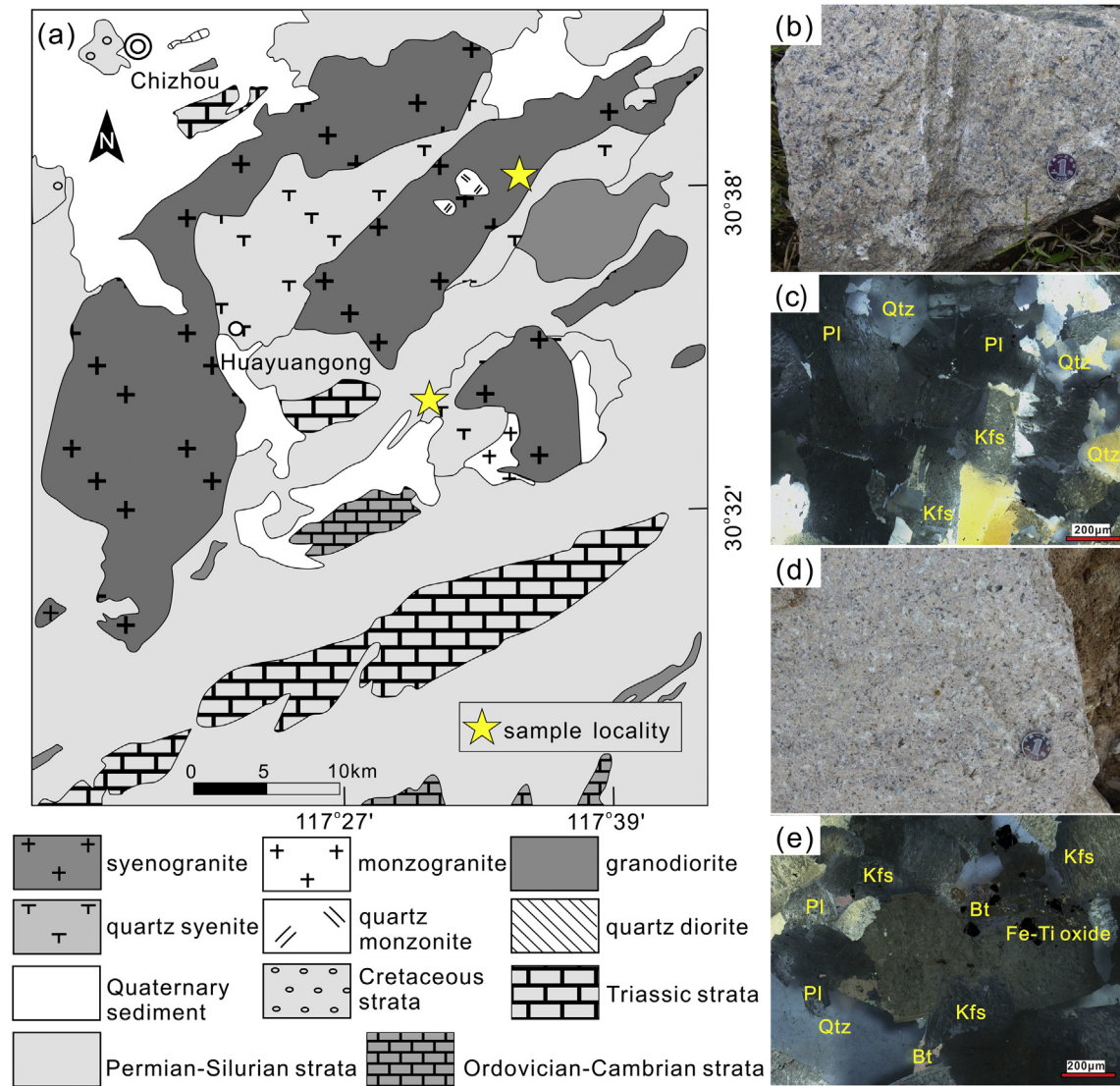
Fig.2. (a)Simplified geological map of the HYG body, showing the major rock units and sample localities (after Liu et al., 2012; Wang et al., 2018); (b–e) Field and photomicrographs of the HYG intrusive rocks, (b)field photograph of syenogranite (sample 16HYG01); (c)thin section photograph of syenogranite (sample 16HYG01, cross-polarized light); (d)field photograph of quartz syenite (sample 16HYG07); (e)photomicrograph of quartz syenite (sample 16HYG07, cross-polarized light). Mineral abbreviations: Qtz = quartz, Kfs = potassium feldspar, Pl = plagioclase, Bt = biotite.

Bureau, Shandong, China. During the analytical process, the experiment was conducted using 15 kV, 10 nA, 10 μm defocused beam. The standards used were norbergite for F, Ba$_5$(PO$_4$)$_3$Cl for Cl, and apatite for Ca and P analyses. Fluorine and Cl were analyzed for 10 s in order to avoid volatile loss, and 20 s for other elements. Fluorine and Cl were measured using the Kα line on a LDE1 crystal and a PET crystal, respectively. Analytical precision for most of the major elements is better than 1%, but for F and Cl precision is around 5%.

Minor and trace elements in apatite were determined using a LA-ICP-MS at the State Key Laboratory of Ore Deposit Geochemistry, Institute of Geochemistry, Chinese Academy of Sciences (IGCAS). The Agilent 7700X ICP-MS instrument is coupled to a Resonetics 193 nm ArF excimer laser ablation system. In situ LA-ICP-MS analyses were performed on the same apatite measured by electron microprobe analyses. Ablation protocol employed a spot diameter of 44 μm at 4 Hz repetition rate for 40 s (equating to 160 pulses). Each analysis incorporated a background acquisition for approximately 14 s (gas blank) followed by 35 s of data acquisition. The Ca concentration obtained by electron microprobe analysis was taken as the internal standard. The external standard NIST SRM 610 was analyzed to evaluate the reliability of measurement. NIST glasses 612 and the Madagascar and Durango apatite standards

were repeatedly analyzed to determine the experimental precision. Data reduction was performed on the ICPMSDataCal software (after Liu et al., 2008). The precision for elements is <10% for Mn, Sr, Nb, La, Ce, Pr, and Nd, from 10 to 20% for Y, Zr, Ba, Pb, Th, U and the rest of the REEs (Mao et al., 2016).

Apatite major and trace element compositions are listed in Appendix Table2.

4. Analytical results

4.1. Whole-rock geochemistry

The syenogranite group (SiO$_2$ contents of 74.8–76.6 wt%) has lower Al$_2$O$_3$(11.3–11.4 wt%), Na$_2$O (3.67–3.80 wt%) and K$_2$O (4.69–4.80 wt%), in comparison with the quartz syenite group (SiO$_2$ contents of 66.1–66.9 wt%) which has Al$_2$O$_3$ of 16.3–16.6 wt%, Na$_2$O of 5.50–5.62 wt% and K$_2$O of 6.19–6.30 wt%. The syenogranites are sub-alkaline, and the quartz syenites are falling into the alkaline area (Fig.4). They are bothmetaluminous with alumina saturation index ASI [=molar Al$_2$O$_3$/(CaO + Na$_2$O + K$_2$O)] varying from 0.94 to 0.98 (Fig.4), and belong to ferroan series in the Fe* [FeOt/(FeOt + MgO)] diagram (Fig.5). In the

Table1
Major (wt%) and trace (ppm) elements data of the HYG pluton.

Sample	16HYG01	16HYG02	16HYG03	16HYG04	16HYG05	16HYG06	16HYG07
Rock type	Syenogranite	Syenogranite	Syenogranite	Syenogranite	Quartz syenite	Quartz syenite	Quartz syenite
Major elements (wt%)							
SiO_2	76.4	75.9	76.6	76.6	66.9	66.2	66.1
TiO_2	0.19	0.19	0.19	0.20	0.44	0.54	0.48
Al_2O_3	11.4	11.3	11.3	11.4	16.3	16.6	16.4
$Fe_2O_3^T$	2.20	2.16	2.09	2.29	2.45	2.47	2.54
MnO	0.10	0.13	0.19	0.01	0.13	0.13	0.13
MgO	0.03	0.06	0.07	0.07	0.26	0.31	0.28
CaO	0.15	0.30	0.20	0.21	0.80	0.88	0.69
Na_2O	3.80	3.69	3.67	3.75	5.50	5.63	5.42
K_2O	4.72	4.76	4.69	4.80	6.19	6.30	6.26
P_2O_5	0.01	0.01	0.01	0.01	0.04	0.05	0.04
L.O.I.	0.47	0.56	0.53	0.35	0.58	0.58	0.67
Total	99.5	99.1	99.5	99.8	99.6	99.7	99.0
Trace elements (ppm)							
Sc	3.31	4.02	3.98	4.19	8.42	8.84	7.73
V	4.87	4.60	3.96	4.63	18.9	20.1	19.2
Cr	0.46	0.27	0.30	0.37	0.51	0.56	1.99
Ga	30.0	29.4	29.3	29.7	22.8	23.5	23.1
Rb	444	450	472	467	124	128	127
Sr	5.86	4.81	6.21	6.97	46.1	45.8	41.0
Y	74.9	82.0	76.9	104	91.4	115	105
Zr	769	1016	978	622	660	823	720
Nb	74.2	89.3	104	92.7	30.8	36.5	34.5
Cs	1.27	2.22	1.64	1.27	1.83	1.87	1.57
Ba	7.80	9.63	9.55	8.29	210	210	183
La	41.1	41.6	47.1	45.1	153	170	138
Ce	79.8	81.7	94.4	90.3	309	355	295
Pr	7.48	7.78	9.17	8.67	33.3	39.4	32.7
Nd	22.5	23.5	28.3	26.2	116	140	116
Sm	5.27	5.46	6.50	6.26	21.6	27.4	21.8
Eu	0.36	0.40	0.43	0.44	1.67	2.03	1.59
Gd	5.76	5.81	6.93	7.13	17.3	22.3	19.0
Tb	1.27	1.30	1.41	1.65	2.89	3.67	3.13
Dy	9.19	9.66	10.0	12.6	17.6	22.2	20.0
Ho	2.12	2.28	2.30	2.94	3.23	4.22	3.76
Er	7.60	8.25	8.08	10.9	9.63	12.0	10.9
Tm	1.41	1.58	1.53	1.91	1.33	1.67	1.53
Yb	10.3	11.5	11.3	13.9	8.28	10.2	9.51
Lu	1.65	1.88	1.80	2.22	1.19	1.43	1.34
Hf	24.8	31.5	32.3	20.4	14.7	17.7	16.4
Ta	4.69	5.34	6.76	5.87	2.08	2.57	2.39
Pb	40.7	27.6	91.6	52.8	16.6	17.1	16.4
Th	61.1	48.5	57.1	53.3	17.9	18.4	20.7
U	13.2	12.1	18.8	15.1	3.11	3.56	4.34

K_2O vs SiO_2 diagram, they plot into the high-Kcalc-alkaline field and shoshonitic field, respectively. In the MALI ($Na_2O + K_2O$-CaO) diagram, syenogranite samples fall in the alkali-calcic field, and quartz syenites in the alkalic one (Fig.5).

The syenogranite group display different Chondrite-normalizedREE patterns from the quartz syenite group (Fig.6). The syenogranites show 'V-shaped' chondrite-normalizedREE patterns with low $(La/Yb)_N$ ratios (2.33–2.99) and strongly negative Eu anomalies (δEu = 0.19–0.21) (Fig.6a). In contrast, the quartz syenites display LREE-enriched patterns with higher $(La/Yb)_N$ ratios (10.4–13.3) and δEu values (0.23–0.26) (Fig.6a). In the primitive mantle-normalized trace element spider diagram (Fig.6b), the HYG granites all show enrichment in Rb, Th, U and LREE and relative depletion in Ti, Ba, Sr, Eu and P. It is noted that the syenogranite group has more depleted Ti, Ba, Sr, Eu and P compared with the quartz syenite group, and exhibits no Nb-Ta depletion (Fig.6b). They all show high Ga/Al ratios (10,000 × Ga/Al = 4.91–4.96 for the syenogranites 2.64–2.68 for the quartz syenites) and Zr + Nb + Ce + Y concentrations (909–1269 ppm for the syenogranites and 1092–1329 ppm for the quartz syenites).

Fluorine contents in the studied rocks vary from 600 to 2010 ppm. The syenogranites have higher F contents (from 1030 to 2010 ppm) than the quartz syenites (from 600 to 760 ppm) (Table1).

4.2. Zircon O-Hf isotopic compositions

Thirty-five zircon grains from the studied granite samples were selected for in-situ oxygen isotopic analyses (Fig.3). They have $\delta^{18}O$ values between 4.7‰ and 7.8‰ (Table2). The syenogranite (16HYG01) has lower values of zircon $\delta^{18}O$ from 4.7‰ to 6.0‰, compared with quartz syenite (16HYG07) with the zircon $\delta^{18}O$ values ranging from 7.0‰ to 7.8‰ (Fig.7). Forty-three zircon grains were analyzed for in-situ Hf isotope (Fig.3). Zircon grains from syenogranite (16HYG01) have weakly negative $\varepsilon_{Hf}(t)$values, ranging from −1.5 to −3.6, but obviously differ from quartz syenite (16HYG07) varying from −3.3 to −6.9.

4.3. Whole-rock Nd isotopic composition

Four whole-rock samples were analyzed for their Nd isotopic compositions. Two syenogranites display nearly same $^{147}Sm/^{144}Nd$ (0.140–0.141) and $^{143}Nd/^{144}Nd$ (0.51232) ratios. Calculated initial ε_{Nd} (t)values are −5.30 to −5.36. The quartz syenite yield different Nd isotopic compositions from the syenogranites, with $^{147}Sm/^{144}Nd$ = 0.118–0.114 and $^{143}Nd/^{144}Nd$ = 0.51219. The initial $\varepsilon_{Nd(t)}$ values are −7.42 to −7.52.
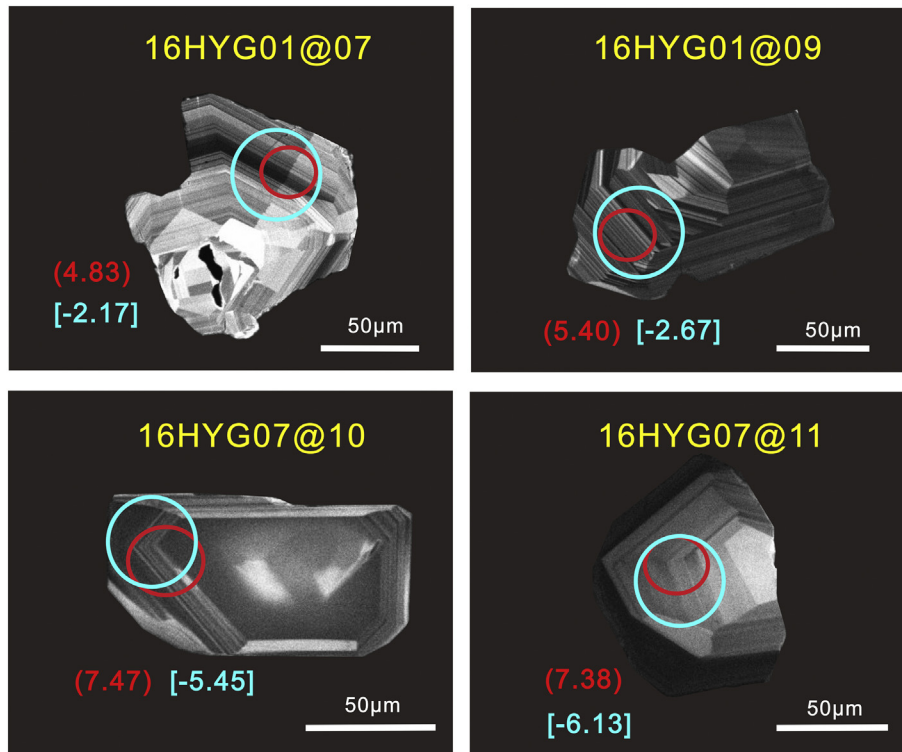
Fig.3. Cathodoluminescence images of representative zircon grains analyzed for O and Lu-Hf isotopes of the HYG A-type granites. The red circles indicate the analytical areas for SIMS O-isotopes, and the large blue circles denote the LA-MC-ICPMS analytical spots for Lu-Hf isotopes. Numbers near the analytical spots are the $\delta^{18}O$ values (within parentheses) and ε_{Hf} (t)values [within square brackets].

4.4. Apatite major and trace element compositions

All apatite grains are fluorapatite and mostly intact prismatic crystals with smooth surface, which are typical for igneous apatite. Apatite grains from the quartz syenite have relatively high F and low Cl concentrations, with F contents varying from 2.52 to 4.12 wt%, and Cl contents from b.d.l. (below the detection limit) to 0.03 wt%. The apatite grains contain low MnO contents from 0.26 wt% up to 0.53 wt%, but low MgO ≤ 0.05 wt%, and FeO ≤ 0.13 wt%. They have right inclined, LREE-enriched chondrite normalized REE patterns, with high $(La/Yb)_N$ ratios (8.2 to 33.8) and strong negative Eu anomalies (0.10 to 0.32).

5. Discussions

5.1. Petrogenetic type: A-type affinity

Loiselle and Wones (1979) introduced the term "A-type granite" to represent granitic rocks with characteristic high alkaline concentrations, high Ga/Al ratios, enrichments in Nb, Ta, Zr and Hf, and high magmatic temperature (Collins et al., 1982; Whalen et al., 1987). A number of geochemical classification schemes have been put forward to distinguish A-type from other types of granites (Eby, 1990; Frost et al., 2001; Whalen et al., 1987). Eby (1992) divided A-type granite into two sub-types (A_1 and A_2) with different origins and tectonic backgrounds. A_1-type granites have chemical characteristics similar to those observed for oceanic island basalts and are emplaced in intraplate setting (Eby, 1992). Whereas, A_2-type granites have geochemical affinities similar to island arc basalts, which are developed at convergent margins (Eby, 1992). Some researchers proposed oxidized and reduced subgroups to stress the significance of redox state and water content in the formation of A-type granites (Anderson and Morrison, 2005; Dall'Agnol and Oliveira, 2007). They proposed that oxidized A-type magmas were derived from melts with appreciable H_2O contents

(≥4 wt% H_2O). Reduced A-type granites are suggested to be derived from sources with low H_2O contents (2–3 wt%) (Dall'Agnol and Oliveira, 2007; Patiño Douce, 1997 and references therein).

The characteristic interstitial nature of the mafic phases of HYG granites (Fig.2) is unique for A-type granite (Collins et al., 1982). Moreover, the characteristic high FeOt/MgO ratios (10.5 to 26.4), high K_2O + Na_2O (8.36 wt%–8.55 wt% and 11.7 wt%–11.9 wt%), high field strength elements (Zr + Nb + Ce + Y = 909 ppm–1269 ppm and 1092 ppm–1329 ppm) and high Ga/Al ratios (10,000 × Ga/Al = 4.91–4.96 and 2.64–2.68), also suggest an A-type affinity (Fig.9a and b). Samples in this study are plotted in the "within-plate granite" field in the diagrams of Pearce et al. (1984)(Fig.8) and in the field of "A-type granites" in the discrimination diagrams of Whalen et al. (1987). According to the three-fold subdivision of Eby (1992), syenogranites belong to the A_1sub-group, and quartz syenites belong to the A_2sub-group(Fig. 9c and d). Furthermore, based on the discrimination diagrams proposed by Dall'Agnol and Oliveira (2007), the A_1 subgroup falls into the reduced A-type granite field, and A_2subgroup belong to the oxidized part (Fig. 9e and f).

5.2. Estimation of physical and chemical properties

Physico-chemical conditions, such as temperature, redox state and water content, play an important role in the granite petrogenesis and evolution. Magmatic temperature has significant implications for the granite petrogenesis. Whole-rock zircon saturation thermometry (T_{Zr}) is generally used to constrain magma temperatures. Based on the equation proposed by Watson and Harrison (1983), the calculated T_{Zr} values of A-type granites vary from 897 to 972 °C (the A_1sub-group 917 to 972 °C, the A_2sub-group 897 to 917 °C). Boehnke et al. (2013) improved the experimental design and computation methods and proposed a new formula for zircon saturation thermometry. The calculated zircon saturation temperature from this new formula is probably a better

Table 2
In-situ zircon O-Hf isotopic data of the HYG pluton.

Spot#	Age (Ma)	$^{176}Lu/^{177}Hf$	2σ	$^{176}Hf/^{177}Hf$	2σ	$\varepsilon_{Hf}(t)$	$\delta^{18}O/‰$	2σ
16HYG01-01	125	0.000683	0.000013	0.282654	0.000008	−1.5	4.88	0.25
16HYG01-02	125	0.001455	0.000012	0.282619	0.000009	−2.8	5.06	0.19
16HYG01-03	125	0.000477	0.000010	0.282633	0.000010	−2.2	5.57	0.18
16HYG01-04	125	0.000157	0.000001	0.282643	0.000009	−1.8	5.53	0.21
16HYG01-05	125	0.003229	0.000003	0.282625	0.000010	−2.7	5.97	0.22
16HYG01-06	125	0.002344	0.000003	0.282617	0.000010	−2.9	5.72	0.21
16HYG01-07	125	0.001587	0.000003	0.282637	0.000009	−2.2	4.83	0.22
16HYG01-08	125	0.005455	0.000008	0.282635	0.000011	−2.5	5.00	0.23
16HYG01-09	125	0.002141	0.000004	0.282624	0.000010	−2.7	5.40	0.24
16HYG01-10	125	0.000442	0.000003	0.282629	0.000011	−2.4	4.97	0.18
16HYG01-11	125	0.002737	0.000004	0.282615	0.000009	−3.0	5.35	0.18
16HYG01-12	125	0.000163	0.000003	0.282605	0.000010	−3.2	4.91	0.25
16HYG01-13	125	0.002899	0.000005	0.282622	0.000009	−2.8	5.02	0.23
16HYG01-14	125	0.003331	0.000010	0.282628	0.000011	−2.6	4.98	0.27
16HYG01-15	125	0.000067	0.000000	0.282611	0.000010	−3.0	5.68	0.17
16HYG01-16	125	0.004264	0.000006	0.282604	0.000011	−3.6	4.99	0.27
16HYG01-17	125	0.000736	0.000007	0.282628	0.000010	−2.4	4.95	0.24
16HYG01-18	125	0.001392	0.000005	0.282620	0.000010	−2.8	4.72	0.21
16HYG01-19	125	0.000717	0.000001	0.282619	0.000010	−2.7		
16HYG01-20	125	0.000953	0.000003	0.282623	0.000009	−2.6		
16HYG01-21	125	0.000903	0.000003	0.282627	0.000009	−2.5		
16HYG07-01	125						7.46	0.23
16HYG07-02	125	0.002564	0.000014	0.282540	0.000009	−5.7	7.69	0.24
16HYG07-03	125	0.001922	0.000011	0.282509	0.000011	−6.7	7.21	0.26
16HYG07-04	125	0.002172	0.000027	0.282506	0.000010	−6.9	7.00	0.24
16HYG07-05	125	0.003534	0.000003	0.282518	0.000011	−6.5	7.08	0.23
16HYG07-06	125	0.001595	0.000010	0.282518	0.000012	−6.4	7.38	0.23
16HYG07-07	125	0.001641	0.000004	0.282503	0.000011	−6.9	7.25	0.25
16HYG07-08	125	0.002378	0.000002	0.282510	0.000011	−6.7	7.37	0.19
16HYG07-09	125	0.001636	0.000003	0.282544	0.000012	−5.5	7.17	0.19
16HYG07-10	125	0.001636	0.000003	0.282544	0.000012	−5.5	7.47	0.18
16HYG07-11	125	0.001275	0.000001	0.282524	0.000011	−6.1	7.38	0.17
16HYG07-12	125	0.003917	0.000002	0.282601	0.000013	−3.6	7.31	0.29
16HYG07-13	125	0.002901	0.000095	0.282518	0.000012	−6.5	7.14	0.17
16HYG07-14	125	0.003079	0.000008	0.282596	0.000013	−3.8	7.27	0.25
16HYG07-15	125	0.001420	0.000002	0.282561	0.000011	−4.8	7.45	0.21
16HYG07-16	125	0.001724	0.000005	0.282566	0.000011	−4.7	7.47	0.22
16HYG07-17	125	0.003841	0.000031	0.282520	0.000013	−6.5	7.83	0.16
16HYG07-18	125	0.003841	0.000031	0.282530	0.000013	−6.1		
16HYG07-19	125	0.002578	0.000004	0.282588	0.000011	−4.0		
16HYG07-20	125	0.002264	0.000001	0.282607	0.000012	−3.3		
16HYG07-21	125	0.003685	0.000013	0.282605	0.000011	−3.5		
16HYG07-22	125	0.002714	0.000010	0.282566	0.000012	−4.8		

estimation of the magma temperature. The calculated T_{Zr} values are 860–964 °C (the syenogranites 896 to 964 °C, the quartz syenites 860 to 882 °C; Fig.5). To be noted is that zircon saturation temperatures calculated from whole rock compositions provide the minimum temperature estimates if the magma was unsaturated in Zr (Miller et al., 2003). No inherited zircons were found in the studied samples, so the magmas that formed these granites were likely unsaturated in Zr and thus their calculated T_{Zr} values are the minimum estimates of their initial

magmatic temperature (Miller et al., 2003), which are consistent with the experimental temperatures at which A-type granitic melts are produced (Patiño Douce, 1997; Skjerlie and Johnston, 1993).

Variations in redox states revealed by minerals, offer an important insight into both the magma source and tectonic settings (e.g.,Foley, 2011; Ishihara, 2004). Zircon incorporates a variety of trace elements during crystallization. Partitioning of Ce^{4+} into the crystal structure is favored relative to Ce^{3+}(Shannon, 1976). The proportion of Ce^{3+}
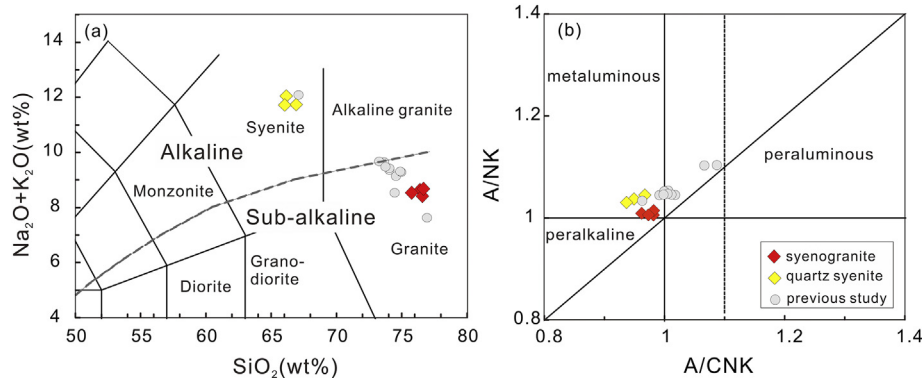

Fig.4. (a)SiO₂ versus K₂O + Na₂O diagram for intrusive rocks; (b)A/NK vs. A/CNK diagram. The HYG granite shows a metaluminous nature. A/NK = Al₂O₃/(Na₂O + K₂O) (molar ratio). A/CNK = Al₂O₃/(CaO + Na₂O + K₂O) (molar ratio). Grey circles stand for data from previous studies of the HYG intrusion by H. Li et al. (2012) and Wang et al. (2018).
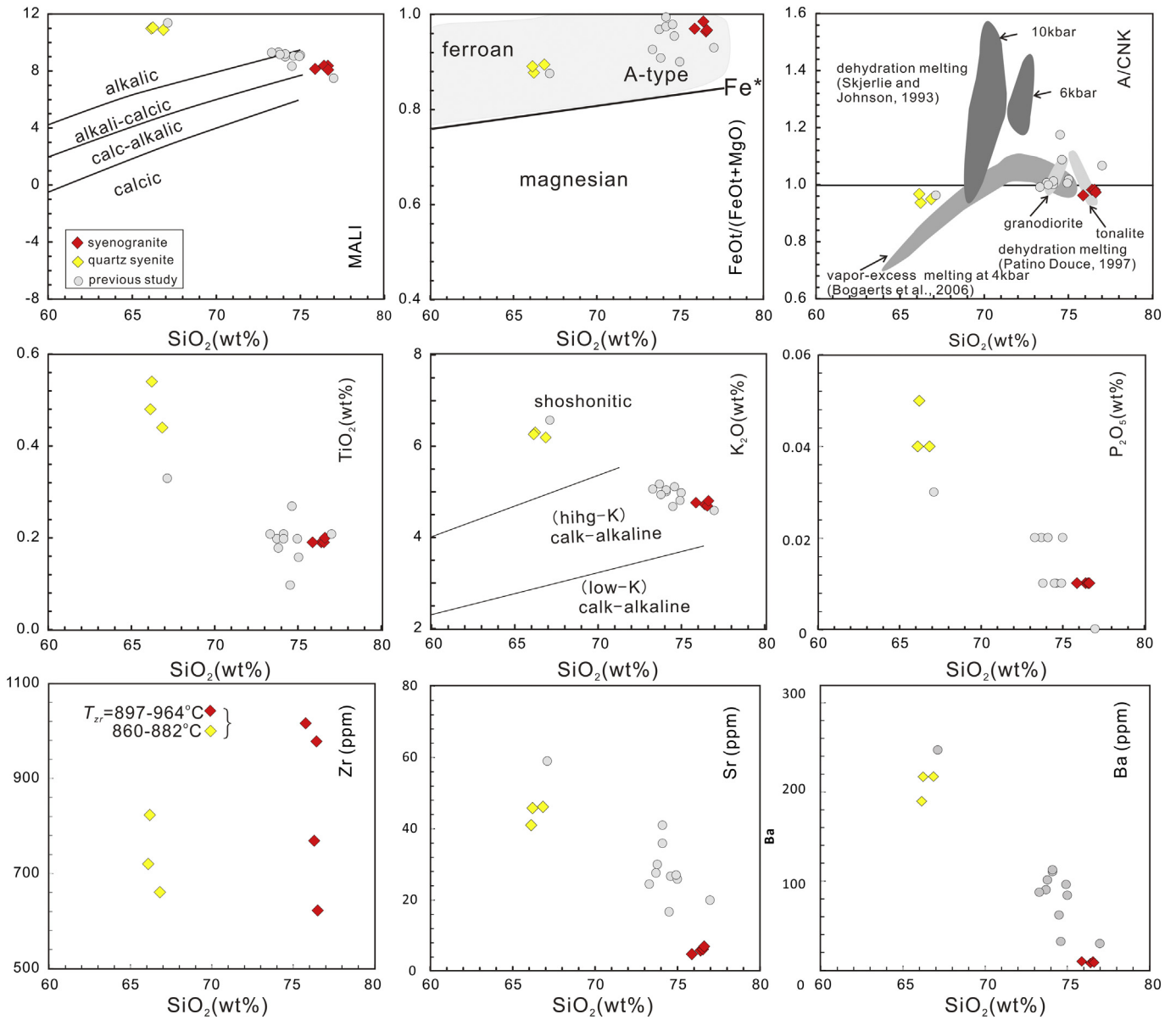
Fig.5. Harker-type major and trace element plots for the HYG A-type granites. Grey circles stand for data from previous studies of the HYG intrusion by H. Li et al. (2012) and Wang et al. (2018).

relative to Ce^{4+} is a function of the oxygen fugacity. Thus, the Ce^{4+}/Ce^{3+} ratio of zircon is a direct indicator of the magma oxidation state (Ballard et al., 2002; Trail et al., 2012). The trace element chemistry of zircons

and the whole-rock compositions of the HYG granites (Li et al., 2012) are used to calculate the Ce^{4+}/Ce^{3+} ratios. These results are mostly lower than 1000 (from 7.33 to 4401) (Appendix Table3). Among these
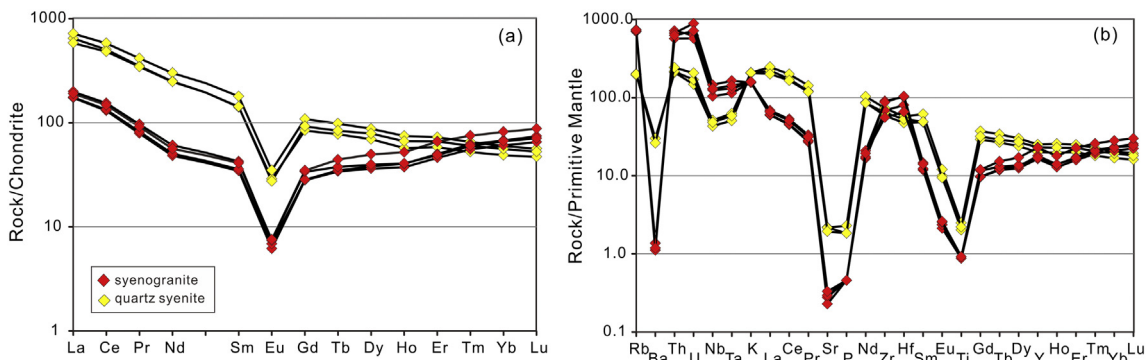
Fig.6. (a)Chondrite-normalized REE diagrams; (b)primitive mantle-normalized trace element spidergrams for the HYG A-type granites. Normalization values are from Sun and McDonough (1989).
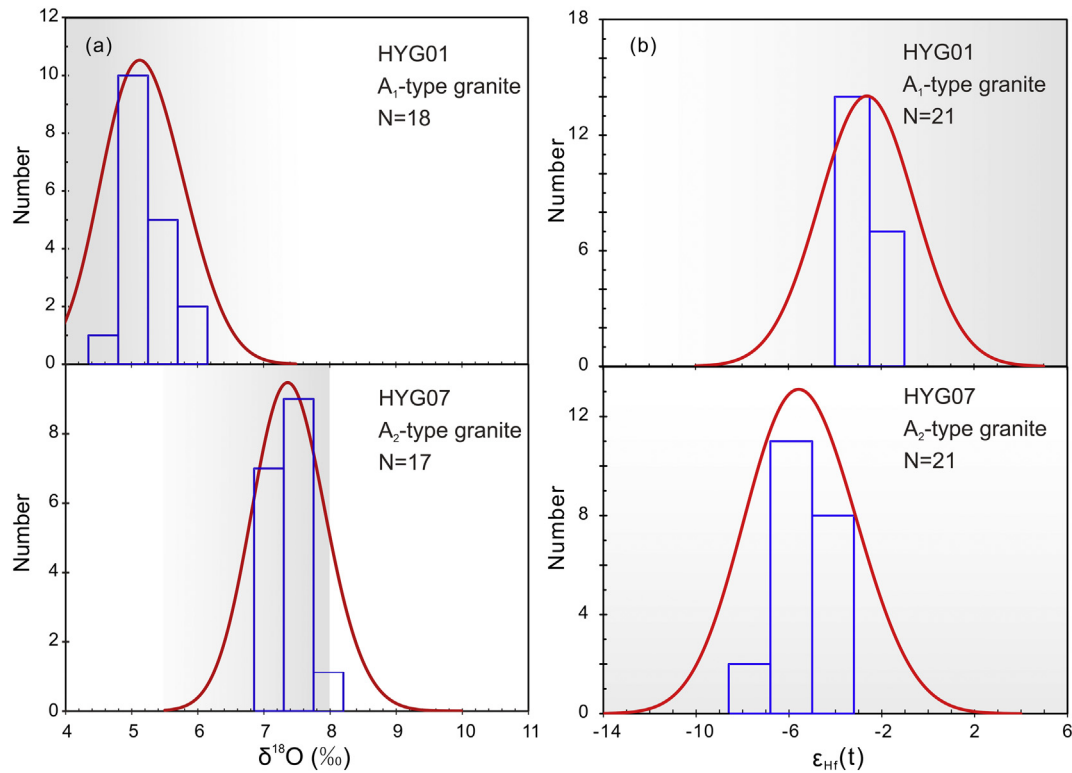
Fig.7. Probabilistic histogram of $\delta^{18}O$ (a) and $\varepsilon_{Hf}(t)$ (b) values for the HYG zircon.

zircons, the Ce^{4+}/Ce^{3+} values for A_1-type granites are systematically lower than those of A_2-type granites, with the average 114 and 950, respectively (Appendix Table3). The zircon Ce anomaly estimation indicates that the A_2-type granites are systematically more oxidized than A_1-type granites, which favors the classification result (Fig. 9e and f).

Magma viscosity (expressed as η) controls the magma transport dynamics and rates of physicochemical processes in natural magmas (Giordano et al., 2008 and reference therein). It is strongly dependent on temperature and dissolved volatile (H_2O and F)contents, hotter and wetter melts have lower viscosity (Giordano et al., 2004). Fluorine is one of the most important volatiles in granitic systems. The presence of F has a great significance for the petrogenesis in F-rich differentiated felsic magmas (Giordano et al., 2004). Low viscosity is a general signature of A-type granitic magmas as indicated by their generally shallow intrusive level, the presence of miarolitic textures and lack of xenoliths or other residual materials from the magma source (Martin, 2006). Whole-rock compositions of the HYGA-type granites (including measured bulk F concentrations and estimated H_2O contents)

combined with zircon saturation temperatures are used to calculate melt viscosities on the basis of the model modified by Giordano et al. (2008). The HYGA-type granites display low magma viscosities, with η values of 10^5–10^6 Pa s for A_1-type granites and 10^4 Pa s for A_2-type granites (Appendix Table4). The negative correlation exists between η and F concentrations within the A_1 and A_2 subgroup. However, no linear relationship is observed within the pluton. This might be influenced by the H_2O contents in the different source areas, for dissolved volatiles exert strong effect on the magmatic viscosity (Giordano et al., 2004).

5.3. The petrogenesis of A-type granites

Although A-type granites are generally formed under extensional tectonic settings, there is no clear consensus on their origin (Bonin, 2007). The petrogenetic models include (1)direct fractionation products of mantle-derived magmas, with or without involvement of crustal rocks (Eby, 1990; Turner et al., 1992); (2)low degree partial melting of
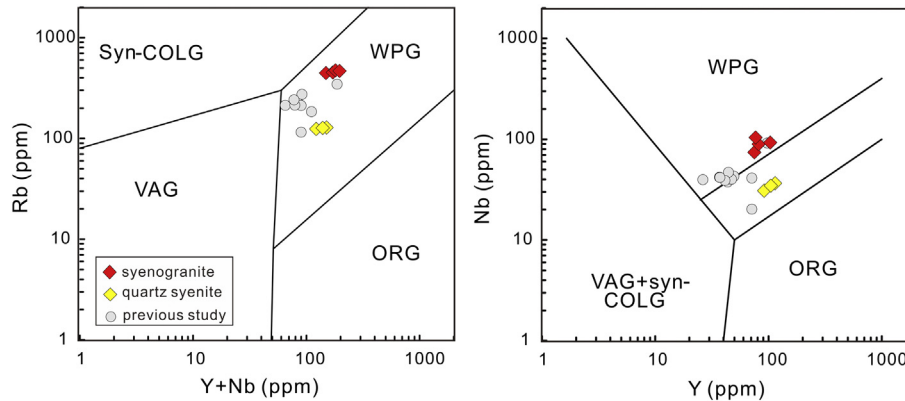

Fig.8. Tectonic discrimination diagrams after Pearce et al. (1984). ORG - ocean ridge granite; VAG - volcanic arc granite; syn-COLG - syn-collision granite; WPG - within-plate granite.
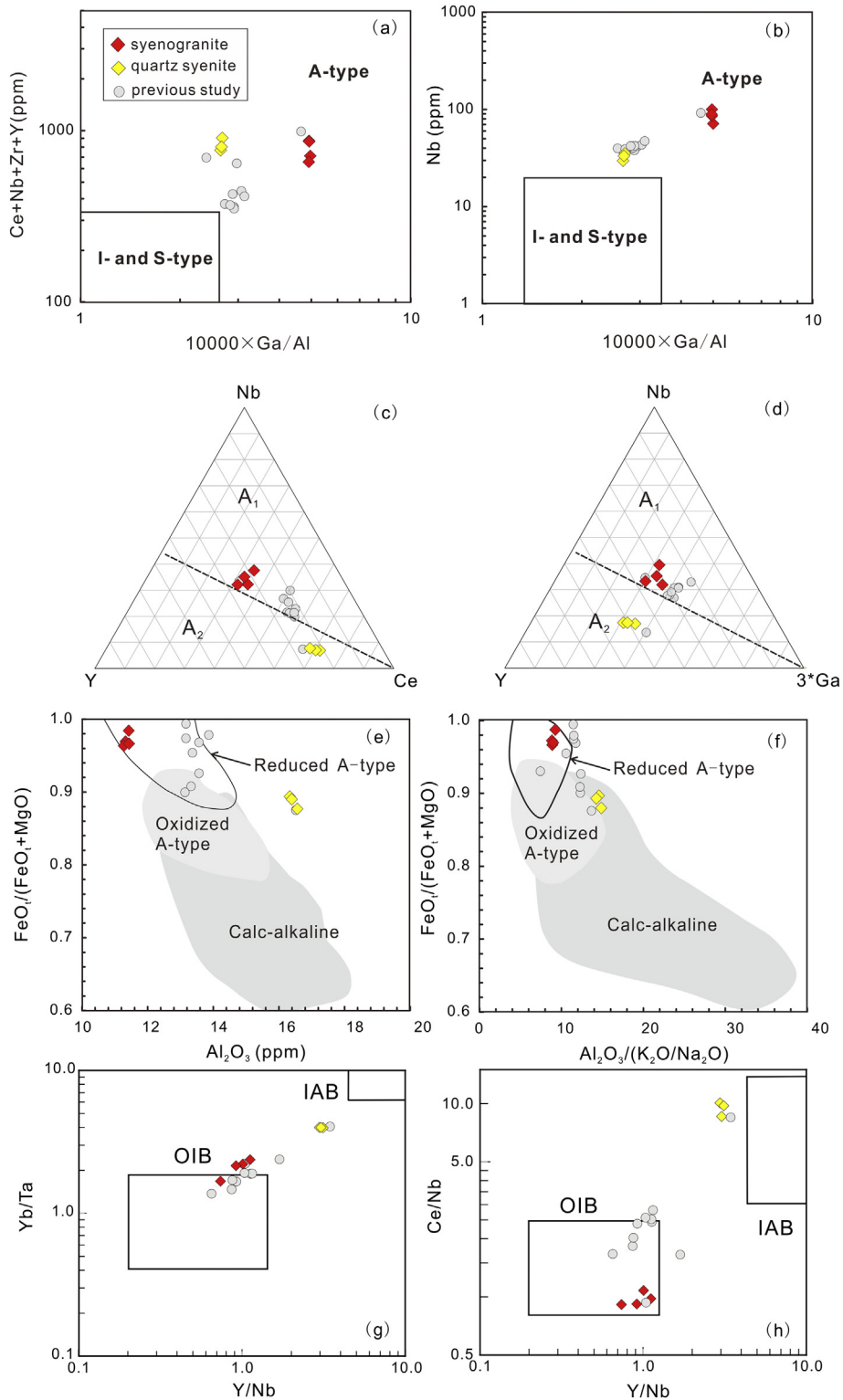
Fig. 9. Discrimination diagrams for A-type granites in the HYG intrusion. (a) and (b) after Whalen et al. (1987); (c), (d), (g) and (h) after Eby (1992); (e) and (f) Dall'Agnol and Oliveira (2007).

lower crustal granulitic residue that were extracted by previous melt (Collins et al., 1982; Landenberger and Collins, 1996; Whalen et al., 1987); (3) anatexis of underplated I-type tonalitic crustal source in the shallow crust level (Creaser et al., 1991; Sylvester, 1989; Skjerlie and Johnston, 1993; Patiño Douce, 1997); (4) crustal melts mixing with mantle-derived mafic magmas (Wickham et al., 1996; Yang et al., 2006).

5.3.1. The origin of A₁-type granites: fractional crystallization of lithospheric mantle derived magma

Zircons in equilibrium with pristine mantle-derived melts have a narrow range of δ¹⁸O (5.3 ± 0.3‰) (1SD, Cavosie et al., 2009; Valley, 2003). This range is constant because the attendant rise in bulk rock δ¹⁸O is compensated for by an increase in zircon/liquid δ¹⁸O fractionation, from
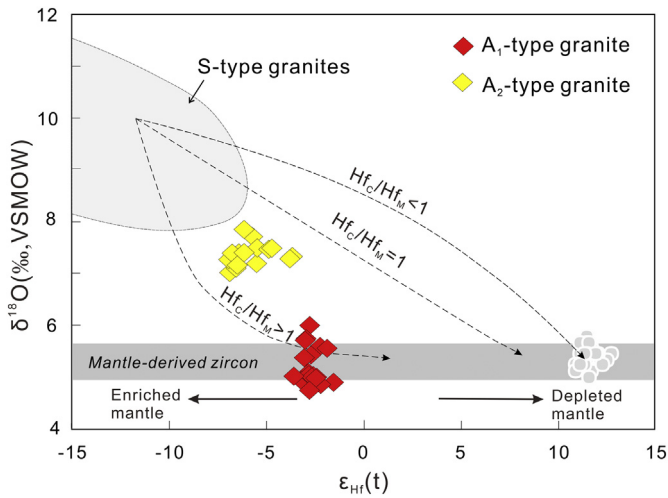
Fig.10. Plot of in-situ zircon $\varepsilon_{Hf}(t)$ and $\delta^{18}O$ of the HYG A-type granites. Mixing lines are drawn to fit data points and to reflect differences in Hf content ratios between crust (C) and mantle (M)derived members. Grey circles are the Qinghu zircons ($\varepsilon_{Hf}(t)$ = 11.6 ± 0.3, $\delta^{18}O$ = 5.4 ± 0.3‰), which are representative end-member values of the mantle sources in South China during the Late Mesozoic (Li et al., 2009). Hafnium-oxygen space of "S-type zircons" is after Kemp et al. (2007). The "mantle zircon" value is after Valley et al. (2005). VSMOW– Vienna standard mean ocean water.

+0.5‰ for mafic melts to +1.5‰ for silicic derivatives (Valley, 2003). Values of $\delta^{18}O$ in zircon that significantly deviate from the limited range (5.3 ± 0.3‰) fingerprint an ^{18}O-enriched supracrustal component (Eiler, 2001) or an ^{18}O-depleted hydrothermally altered component involved in the magma from which the zircon crystallized. Some studies proposed that <1‰ variations of $\delta^{18}O_{Zrn}$ could be the result of parental-melt compositions and crystallization temperature (Bindeman and Valley, 2001; Grimes et al., 2011; Zhao and Zheng, 2003). Moreover, the uncertainty of 0.1–0.2‰ (1SD) exists for SIMSzircon O-isotope measurement should also be taken into account (Tang et al., 2015), a slight "depletion" in $\delta^{18}O$ compared to mantle values (5.3 ± 0.3‰) might not indicate interaction with hydrothermal fluids (Gao et al., 2017). Granites with $\delta^{18}O_{Zrn}$ of <4.6–4.7‰ (95% confidence level) can be considered to be "low-$\delta^{18}O$" ones (Gao et al., 2017). Thus, $\delta^{18}O$ values of A_1-type granite (ranging from 4.7‰ to 6.0‰) are roughly overlap with mantle values, indicating rare involvement of "low-$\delta^{18}O$" components.

According to Eby (1992), the A_1-type granite is supposed to be formed by differentiation of magmas like those of oceanic-island basalts. Reduced A-type granite is thought to be derived from tholeiitic rocks or quartz-feldspathic igneous sources (e.g.,Dall'Agnol and Oliveira, 2007; Frost and Frost, 1997; Patiño Douce, 1997) or the high-

temperature melting of granulitic metasedimentary rocks (Huang et al., 2011). Themantle-like oxygen values of HYG A_1-type granite preclude the possibility of metasediments as the dominant source material.

Enriched mantle source of the HYG A_1-type granite is also supported by both trace element as well as zircon Hf isotopic compositions. The samples plot in the OIB field in the Yb/Ta versus Y/Nb and Ce/Nb versus Y/Nb diagrams (Fig. 9g and h). The higher Nb (74.2 to 104 ppm) and Ta (4.69 to 6.76 ppm) contents and lack of Nb-Ta depletion (Fig.6b) support that the magma was derived from an enriched mantle and rare crustal involvement. The slightly negative $\varepsilon_{Hf}(t)$values (−1.5 to −3.6) and $\varepsilon_{Nd}(t)$values (−5.30 to −5.36) also favor the enriched source component for the A_1-type granite (Fig.10), and the low Y/Nb ratios (0.74 to 1.12) indicate little crustal involvement. Recent studies show that the Late Mesozoic lithospheric mantle under the LYRB was enriched, which is characterized by Sr-Nd-Pb isotopic enrichment (e.g.,Ling et al., 2009; Ling et al., 2011; Wang et al., 2013).

A recent study by Gao et al. (2017) proves that the fractional crystallization plays an important role in producing the slightly low $\delta^{18}O$ signature. The trend of ^{18}O during magmatic evolution is dependent on the type of and sequence of mineral crystallizing, which is controlled bythe magma composition and physic-chemical conditions (Taylor, 1968). The low water content of the reduced A-type granites suppressed the biotite and hornblende crystallization. And the low f_{O2} is responsible for minor precipitation of magnetite. Those two factors cause the slightly depleted ^{18}O. The very low MgO, CaO, Al_2O_3, Sr, Ba and Eu with high SiO_2 infer that the HYG A_1-type granite experienced highly fractional crystallization, which is also supported by their extremely high Rb/Sr ratios (up to 94) (Halliday et al., 1991). Thus, a ferrogabbro-type fractional crystallization may be responsible for producing the geochemical characteristics and oxygen isotope variations, as well as ~0.5‰ $\delta^{18}O$ depletion in A_1-type granite.

Thus, integrated the mantle-like $\delta^{18}O_{Zrn}$ ratios, enriched isotopic compositions and geochemical characteristics, the HYG A_1-type granite is most likely produced by intensive ferrogabbro-type fractionation ofreduced, anhydrous basaltic melts derived from the enriched lithospheric mantle (Fig.11).

5.3.2. The origin of A_2-type granites: contributions from metasomatized lithospheric mantle

The $\delta^{18}O$ values of A_2-type granite zircons are lower than 8‰, precluding the possibility of metasediments as the dominant source materials. The unimodal distribution of the zircon O-Hf isotope does not support a hybrid model (Fig.7). Relatively lower SiO_2 contents (< 67 wt%) are not consistent with the dehydration melting of calc-alkaline granitoids in the shallow crust, which produces the high-silica metaluminous A-type granites (Patiño Douce, 1997). Partial melting of
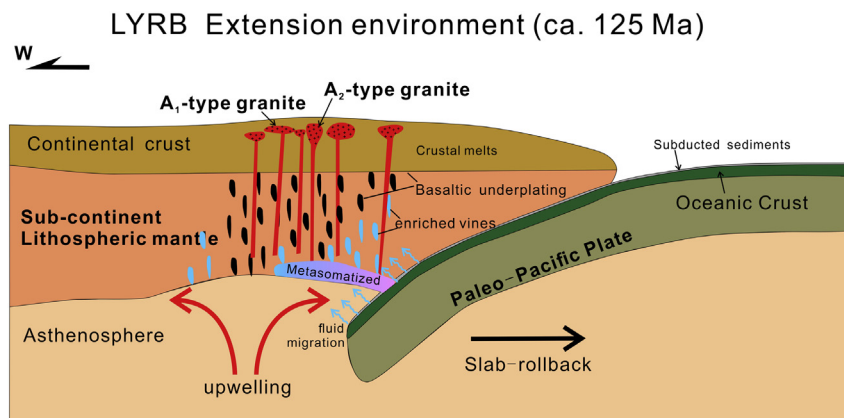

Fig.11. Cartoon illustrating synchronous formation of A_1- and A_2-type granites in the LYRB, eastern China. The upward migration of fluids/melts offers a very efficient mechanism of transfer components into the overlying lithospheric mantle, the proportion of which is of primordial importance in the nature of the melting reactions. The metasomatic step leading up to partial melting has caused a major enrichment in high field-strength elements, including the rare earths, and these patterns of enrichment are reflected in the magmas produced.

granulitic residue from which a granitic melt had previously been extracted is also not suitable for the A$_2$-type granites. Because experimental results show that melts produced by partial melting of refractory granulitic residues are depleted in alkalis (Creaser et al., 1991; Patiño Douce, 1997). Here, we contend that the HYG A$_2$-type granites are originated from the partial melting of the metasomatized mantle.

The calculated F and Cl concentrations of the magma, on the basis of apatite compositions and partition coefficients (D$_F^{ap/melt}$ = 23.8, D$_{Cl}^{ap/melt}$ = 1.3; Webster et al., 2009), are 995 to 1280 ppm and 0 to 231 ppm, respectively. While, F and Cl abundances in primitive mantle are estimated at 25 and 17 ppm, respectively (e.g., McDonough and Sun, 1995), and an order of magnitude higher in the average continental crust (553 and 244 ppm, respectively; Rudnick and Gao, 2003). Moreover, the crystallization of apatite cannot lead to a strong enrichment or depletion of Cl in granitic melts, indicating constant Cl concentration over a large temperature range. Similarly, F concentrations derived from apatite compositions do not change significantly within the crystallization interval (Zhang et al., 2012). Thus, there must be other geological processes responsible for the high volatile components in the source areas. Recent study suggests that the breakdown of minerals during partial melting of subducted oceanic crust makes important contributions to the volatile components in A-type granites (Jiang et al., 2018).

The A$_2$-type granites have high potassium contents (K$_2$O/Na$_2$O = 1.1–1.5) and enriched Sr-Nd and Hf isotopic compositions (I_{Sr}(t) = 0.7072–0.7084, ε$_{Nd}$(t) = −7.46−−7.67 and ε$_{Hf}$(t) = −3.3−−6.9; (Wang et al., 2018) and this study), which are similar to the magmatic rocks derived from the lithospheric mantle (Xie et al., 2011; Xing, 1998; Yan et al., 2008; Yan et al., 2015). The higher zircon δ^{18}O values (7.0‰–7.8‰) than the mantle value 5.3 ± 0.3‰ (Valley et al., 2003), indicating some kind of high δ^{18}O materials in the source of A$_2$-type granites. However, they are clearly lower than melts of basaltic rock and/or sediments in the upper part of the oceanic crust (δ^{18}O values about 9‰ to 20‰), and also higher than melts derived from hydrothermally altered gabbros from the interior of the oceanic crust (δ^{18}O values of approximately 2‰ to 5‰) (Bindeman et al., 2005). The addition of terrigenous sediment in subduction zone into the magma source may be an important candidate that cause an increase in K$_2$O/Na$_2$O, ^{87}Sr/^{86}Sr ratios, δ^{18}O values, f_{O2} and a decrease in ε$_{Hf}$(t)and ε$_{Nd}$(t)values (Wang et al., 2013). The island-arc chemical characteristics for the whole-rock compositions of the A$_2$-type granites might be introduced through subduction-released fluids (Chen et al., 2016; Li et al., 2012; Li et al., 2014). Therefore, the A$_2$-type granites are supposed to have been formed by partial melting of the lithospheric mantle which was fertilized by subduction slab-derived fluids/melts (Fig.11).

Overall, the studies on the Cretaceous A-type granites in the LYRB imply that alternative distributions of A$_1$- and A$_2$-type granites along the bank are attributed to partial melting of lithospheric mantle with rare metasomatism and enriched lithospheric mantle which was metasomatized by slab derived fluids/melts, respectively (Jiang et al., 2018; Li et al., 2012).

5.4. Geodynamic model for the generation of HYGA-type granites

A-type granites generally develop in extensional tectonic environments regardless of the origin of the magma source (Eby, 1992; Turner et al., 1992; Whalen et al., 1987). Integrating the observations with previous studies, we envisage a geodynamic model to link the petrogenesis of the HYGA-type granite and other Late Cretaceous A-type granites in the LYRB to the ridge subduction between the Pacific and Izanagi Plates (e.g., Jiang et al., 2018; Li et al., 2012; Ling et al., 2009).

In the late Early Cretaceous (after ca. 130 Ma), slab-rollback due to the changes of plate movement direction and the angle of the Paleo-Pacific Plate subduction (e.g., Gu et al., 2017; Li et al., 2012; Sun et al., 2007; Wang et al., 2014; Wu et al., 2017), caused the regional extension and placed the LYRB in a back-arc setting (e.g., Gu et al., 2017; Yan et al., 2015). The widespread of A-type granites (129 to 120 Ma) (e.g., Li et

al., 2012; Xing and Xu, 1994), the coeval shoshonites and volcanic rocks, and the development of expanding basins, all clearly denote such extensional tectonic regime (e.g., Ling et al., 2009; Sun et al., 2007; Wang et al., 2014; Xie et al., 2011; Yan et al., 2015). The higher magma temperature conditions for the younger magmatic events indicates an increasing heat supply from the upwelling asthenosphere and an increasing intensity of extensional activity, which are also supported by the numerical modeling results (Zhao et al., 2016). The regional extension and the upwelling asthenospheric mantle-derived melt triggered thepartial melting of the metasomatizing lithospheric mantle (by slab-derived fluid/melts) (Li et al., 2012; Ling et al., 2009; Wang et al., 2013). After partial melting of the lithospheric mantle, the initial magma ascended and stalled in the continental upper crust. The initial magmas may be heterogeneous in terms of chemical and isotopic compositions with addition of various amounts of sediments/fluids to their igneous source (Wang et al., 2013). The magma chamber in the middle-upper crust provided the environment for magmas to further evolve (Fig.11). The ultimately developed A$_1$- and A$_2$-type granites belts are roughly parallel to each other. As explained by H. Li et al. (2012), the influence of subduction released fluids decreases from the ridge outward. HYG was likely located near the transition from A$_1$- to A$_2$-type granites. Therefore, A$_1$- to A$_2$-type granites coexist in this single pluton.

In summary, the metasomatism and decompression of lithospheric mantle, and later fractional crystallization play critical roles in the formation of HYGA-type granites as well as A-type granites developed in the LYRB. A$_1$-type granites were derived from the enriched lithospheric mantle where was hot, reduced and dry, in contrast to the A$_2$-type granites which were originated from partial melting of lithospheric mantle metasomatized by slab derived fluids/melts during the subduction process.

6. Conclusions

1) The HYG granites are characterized by high alkali, high HFSEconcentrations and elevated Ga/Al ratios, indicative of an A-type affinity. According to the whole-rock geochemical compositions, the HYG pluton can be further divided into A$_1$- and A$_2$-typesubgroups that are also reduced and oxidized A-type granite, respectively. These two subgroups not only display different whole-rock geochemical signatures but also are formed under diverse physico-chemical conditions. The A$_1$-type granites are formed under hot, reduced and dry conditions, compared to the relatively cold, oxidized and wet setting for the A$_2$-type ones.

2) In-situ zircon O-Hf isotope compositions of HYG A$_1$- (δ^{18}O = 4.7‰–6.0‰, ε$_{Hf}$(t) = −1.5−−3.6) and A$_2$- (δ^{18}O = 7.0‰–7.8‰, ε$_{Hf}$(t) = −3.3−−6.9) subgroups suggest different source materials for them in the single one pluton. The mantle-like δ^{18}O ratios and negative ε$_{Hf}$(t)values of A$_1$-type granites indicate an enriched lithospheric mantle source. The whole-rock geochemical characteristics suggest fractionation plays an important role in the magmatic evolution process. In contrast, the higher δ^{18}O values and more enriched ε$_{Hf}$(t)values of A$_2$-type granites favor the derivation from the partial melting of the lithospheric mantle which are metasomatized by fluids/melts originated from downgoing subducted slab.

3) A$_1$- and A$_2$-type granites can be synchronously formed under the extensional setting with the thinning of lithospheric mantle and upwelling of the asthenosphere. The heterogeneous source components induced by subduction, play a vital role in the formation of coexisting A$_1$- and A$_2$-type granites.

Acknowledgements

Appendix A. Supplementary data

Supplementary data to this article can be found online at https://doi.org/10.1016/j.lithos.2018.08.008.

References

Anderson, J.L., Morrison, J., 2005. Ilmenite, magnetite, and peraluminous Mesoproterozoic anorogenic granites of Laurentia and Baltica. Lithos 80, 45–60.

Ballard, J.R., Palin, J.M., Campbell, I.H., 2002. Relative oxidation states of magmas inferred from Ce(IV)/Ce(III) in zircon: application to porphyry copper deposits of northern Chile. Contributions to Mineralogy and Petrology 144, 347–364.

Bindeman, I.N., Serebryakov, N.S., 2011. Geology, petrology and O and H isotope geochemistry of remarkably O-18 depleted Paleoproterozoic rocks of the Belomorian Belt, Karelia, Russia, attributed to global glaciation 2.4 Ga. Earth and Planetary Science Letters 306, 163–174.

Bindeman, I.N., Valley, J.W., 2001. Low-δ^{18}O rhyolites from Yellowstone: magmatic evolution based on analyses of zircons and individual phenocrysts. Journal of Petrology 42, 1491–1517.

Bindeman, I.N., Eiler, J.M., Yogodzinski, G.M., Tatsumi, Y., Stern, C.R., Grove, T.L., Portnyagin, M., Hoernle, K., Danyushevsky, L.V., 2005. Oxygen isotope evidence for slab melting in modern and ancient subduction zones. Earth and Planetary Science Letters 235, 480–496.

Boehnke, P., Watson, E.B., Trail, D., Harrison, T.M., Schmitt, A.K., 2013. Zircon saturation re-revisited. Chemical Geology 351, 324–334.

Bonin, B., 2007. A-type granites and related rocks: evolution of a concept, problems and prospects. Lithos 97, 1–29.

Cavosie, A.J., Kita, N.T., Valley, J.W., 2009. Primitive oxygen isotope ratio recorded in magmatic zircon from the Mid-Atlantic Ridge. American Mineralogist 94, 926–934.

Chen, L., Zhao, Z.F., Zheng, Y.F., 2014. Origin of andesitic rocks: geochemical constraints from Mesozoic volcanics in the Luzong basin, South China. Lithos 190–191, 220–239.

Chen, Y.X., Li, H., Sun, W.D., Ireland, T., Tian, X.F., Hu, Y.B., Yang, W.B., Chen, C., Xu, D.R., 2016. Generation of Late Mesozoic Qianlishan A2-type granite in Nanling Range, South China: implications for Shizhuyuan W–Sn mineralization and tectonic evolution. Lithos 266–267, 435–452.

Collins, W.J., Beams, S.D., White, A.J.R., Chappell, B.W., 1982. Nature and origin of A-type granites with particular reference to southeastern Australia. Contributions to Mineralogy and Petrology 80, 189–200.

Creaser, R.A., Price, R.C., Wormald, R.J., 1991. A-type granites revisited: assessment of a residual-source model. Geology 19, 163–166.

Dall'Agnol, R., Oliveira, D.C., 2007. Oxidized, magnetite-series, rapakivi-type granites of Carajás, Brazil: implications for classification and petrogenesis of A-type granites. Lithos 93, 215–233.

Dall'Agnol, R., Rämö, O.T., Magalhães, M.S., Macambira, M.J.B., 1999. Petrology of the anorogenic, oxidised Jamon and Musa granites, Amazonian craton: implications for the genesis of Proterozoic A-type granites. Lithos 46, 431–462.

Dall'Agnol, R., Teixeira, N.P., Rämö, O.T., Moura, C.A.V., Macambira, M.J.B., Oliveira, D.C., 2005. Petrogenesis of the Paleoproterozoic, rapakivi, A-type granites of the Archean Carajás Metallogenic Province, Brazil. Lithos 80, 101–129.

Eby, G.N., 1990. The A-type granitoids: a review of their occurrence and chemical characteristics and speculations on their petrogenesis. Lithos 26, 115–134.

Eby, G.N., 1992. Chemical subdivision of the A-type granitoids: petrogenetic and tectonic implications. Geology 20 (7), 641–644.

Eiler, J.M., 2001. Oxygen isotope variations of basaltic lavas and upper mantle rocks. In: Valley, John, Cole, David R. (Eds.), Reviews in Mineralogy and Geochemistry: Stable Isotope Geochemistry. Mineralogical Society of America, Washington, pp. 319–364.

Foley, S.F., 2011. A reappraisal of redox melting in the Earth's mantle as a function of tectonic setting and time. Journal of Petrology 52, 1363–1391.

Frost, C.D., Frost, B.R., 1997. Reduced rapakivi type granites: the tholeiitic connection. Geology 25, 647–650.

Frost, B.R., Barnes, C.G., Collins, W.J., Arculus, R.J., Ellis, D., Frost, C.D., 2001. A geochemical classification for granitic rocks. Journal of Petrology 42, 2033–2048.

Gao, Y.Y., Griffin, W.L., Chu, M.F., O'Reilly, S.Y., Pearson, N.J., Li, Q.L., Liu, Y., Tang, G.Q., Li, X.H., 2017. Constraints from zircon Hf-O-Li isotopic compositions on the genesis of slightly low-δ18O alkaline granites in the Taohuadao area, Zhejiang Province, SEChina. Journal of Asian Earth Sciences https://doi.org/10.1016/j.jseaes.2017.07.025.

Giordano, D., Romano, C., Dingwell, D.B., Poe, B., Behrens, H., 2004. The combined effects of water and fluorine on the viscosity of silicic magmas. Geochimica et Cosmochimica Acta 68 (24), 5159–5168.

Giordano, D., Russell, J.K., Dingwell, D.B., 2008. Viscosity of magmatic liquids: a model. Earth and Planetary Science Letters 27 (1), 123–134.

Grimes, C.B., Ushikubo, T., John, B.E., Valley, J.W., 2011. Uniformly mantle-like δ^{18}O in zircons from oceanic plagiogranites and gabbros. Contributions to Mineralogy and Petrology 161, 13–33.

Gu, H.L., Yang, X.Y., Deng, J.H., Duan, L.A., Liu, L., 2017. Geochemical and zircon U–Pbgeochronological study of the Yangshan A-type granite: insights into the geological evolution in south Anhui, eastern Jiangnan Orogen. Lithos 284–285, 156–170.

Halliday, A.N., Davidson, J.P., Hildreth, W., Holden, P., 1991. Modelling the petrogenesis of high Rb/Sr silicic magmas. Chemical Geology 92, 107–114.

Huang, H.Q., Li, X.H., Li, W.X., Li, Z.X., 2011. Formation of high δ^{18}O fayalite-bearingA-type granite by high temperature melting of granulitic metasedimentary rocks, southern China. Geology 39, 903–906.

Ishihara, S., 2004. The redox state of granitoids relative to tectonic setting and earth history: the magnetite–ilmenite series 30 years later. Earth and Environmental Science Transactions of the Royal Society of Edinburgh 95, 23–33.

Jiang, X.Y., Li, H., Ding, X., Wu, K., Guo, J., Liu, J.Q., Sun, W.D., 2018. Formation of A-type granites in the Lower Yangtze River Belt: a perspective from apatite geochemistry. Lithos 304–307, 125–134.

Kemp, A.I.S., Wormald, R.J., Whitehouse, M.J., Price, R.C., 2005. Hf isotopes in zircon reveal contrasting sources and crystallization histories for alkaline to peralkaline granites of Temora, southeastern Australia. Geology 33, 797–800.

Kemp, A.I.S., Hawkesworth, C.J., Foster, G.L., Paterson, B.A., Woodhead, J.D., Hergt, J.M., Gray, C.M., Whitehouse, M.J., 2007. Magmatic and crustal differentiation history of granitic rocks from Hf-O isotopes in zircon. Science 315, 980–983.

King, P.L., White, A.J.R., Chappell, B.W., Allen, C.M., 1997. Characterization and origin of aluminous A-type granites from the Lachlan Fold Belt, southeastern Australia. Journal of Petrology 38, 371–391.

Landenberger, B., Collins, W.J., 1996. Derivation of A-type granites from a dehydrated charnockitic lower crust: evidence from the Chaelundi Complex, eastern Australia. Journal of Petrology 37, 145–170.

Li, X.H., Liu, D.Y., Sun, M., Li, W.X., Liang, X.R., Liu, Y., 2004. Precise Sm–Nd and U–Pb isotopic dating of the super-giant Shizhuyuan polymetallic deposit and its host granite, Southeast China. Geological Magazine 141, 225–231.

Li, X.H., Li, W.X., Wang, X.C., Li, Q.L., Liu, Y., Tang, G.Q., 2009. Role of mantle-derived magma in genesis of early Yanshanian granites in the Nanling Range, South China: in situ zircon Hf-O isotopic constraints. Science in China Series D: Earth Sciences 52 (9), 1262–1278.

Li, X.H., Li, W.X., Li, Q.L., Wang, X.C., Liu, Y., Yang, Y.H., 2010a. Petrogenesis and tectonic significance of the ~850 Ma Gangbian alkaline complex in South China: evidence from in situ zircon U–Pb dating, Hf–O isotopes and whole-rock geochemistry. Lithos 114, 1–15.

Li, X.H., Long, W.G., Li, Q.L., 2010b. Penglai zircon megacrysts: a potential new working reference material for microbeam determination of Hf–O isotopes and U–Pb age. Geostandards and Geoanalytical Research 34, 117–134.

Li, H., Zhang, H., Ling, M.X., Wang, F.Y., Ding, X., Zhou, J.B., Yang, X.Y., Tu, X.L., Sun, W.D., 2011. Geochemical and zircon U–Pb study of the Huangmeijian A-type granite: implications for geological evolution of the Lower Yangtze River belt. International Geology Review 53, 499–525.

Li, H., Ling, M.X., Li, C.Y., Zhang, H., Ding, X., Yang, X.Y., Fan, W.M., Li, Y.L., Sun, W.D., 2012. A-type granite belts of two chemical subgroups in central eastern China: indication of ridge subduction. Lithos 150, 26–36.

Li, X.H., Li, Z.X., Li, W.X., Wang, X.C., Gao, Y.Y., 2013a. Revisiting the "C-type adakites" of the Lower Yangtze River Belt, central eastern China: in-situ zircon Hf–O isotope and geochemical constraints. Chemical Geology 345, 1–15.

Li, X.H., Tang, G.Q., Gong, B., Yang, Y.H., Hou, K.J., Hu, Z.C., Li, Q.L., Liu, Y., Li, W.X., 2013b. Qinghu zircon: a working reference for microbeam analysis of U-Pb age and Hf and O isotopes. Chinese Science Bulletin 58, 4647–4654.

Li, H., Ling, M.X., Ding, X., Zhang, H., Li, C.Y., Liu, D.Y., Sun, W.D., 2014. The geochemical characteristics of Haiyang A-type granite complex in Shandong, eastern China. Lithos 200–201, 142–156.

Ling, M.X., Wang, F.Y., Ding, X., Hu, Y.H., Zhou, J.B., Zartman, R.E., Yang, X.Y., Sun, W.D., 2009. Cretaceous ridge subduction along the Lower Yangtze River Belt, Eastern China. Economic Geology 104, 303–321.

Ling, M.X., Wang, F.Y., Ding, X., Zhou, J.B., Sun, W., 2011. Different origins of adakites from the Dabie Mountains and the Lower Yangtze River Belt, eastern China: geochemical constraints. International Geology Review 53 (5–6), 727–740.

Liu, Y.S., Hu, Z.C., Gao, S., Günther, D., Xu, J., Gao, C.G., Chen, H.H., 2008. In situ analysis of major and trace elements of anhydrous minerals by LA-ICP-MS without applying an internal standard. Chemical Geology 257, 34–43.

Liu, Y.Y., Ma, C.Q., Lv, Z.Y., Huang, W.P., 2012. Zircon U-Pb age, element and Sr-Nd-Hf isotope geochemistry of Late Mesozoic magmatism from the Guichi metallogenic district in the Middle and Lower Reaches of the Yangtze River Region. Acta Petrologica Sinica 28 (10), 3287–3305 (in Chinesewith English abstract).

Loiselle, M.C., Wones, D.R., 1979. Characteristics and Origin of Anorogenic Granites: Geological Society of America Abstracts with Programs 11 468p.

Mao, M., Rukhlov, A.S., Rowins, S.M., Spence, J., Coogan, L.A., 2016. Apatite trace element compositions: a robust new tool for mineral exploration. Economic Geology 111 (5), 1187–1222.

Martin, R.F., 2006. A-type granites of crustal origin ultimately result from open-systemfenitization-type reactions in an extensional environment. Lithos 91, 125–136.

McDonough, W.F., Sun, S.S., 1995. Chemical evolution of the mantle. Chemical Geology 120, 223–253.

Miller, C.F., Mcdowell, S.M., Mapes, R.W., 2003. Hot and cold granites? Implications of zircon saturation temperatures and preservation of inheritance. Geology 31, 529–532.

Patiño Douce, A.E., 1997. Generation of metaluminous A-type granites by low-pressure melting of calc-alkaline granitoids. Geology 25, 743–746.

Pearce, J.A., Harris, N.B., Tindle, A.G., 1984. Trace element discrimination diagrams for the tectonic interpretation of granitic rocks. Journal of Petrology 25, 956–983.

Rajesh, H.M., 2000. Characterization and origin of a compositionally zoned aluminous A-type granite from South India. Geological Magazine 137, 291–318.

Rudnick, R.L., Gao, S., 2003. Composition of continental crust. In: Holland, H.D., Turekian, K.K., Rudnick, R.L. (Eds.), Treatise on Geochemistry Vol. 3. Elsevier, Oxford, pp. 1–64.

Shannon, R.D., 1976. Revised effective ionic radii and systematic studies of inter-atomic distances in halides and chalcogenides. Acta Crystallographica, SectionB: Structural Science 32, 751–767.

Skjerlie, K.P., Johnston, A.D., 1993. Fluid-absent melting behavior of an F-rich tonalitic gneiss at mid-crustal pressures: implications for the generation of anorogenic granites. Journal of Petrology 34, 785–815.

Sláma, J., Košler, J., Condon, D., Crowley, J.L., Gerdes, A., Hanchar, J.M., Horstwood, M.S.A., Morris, G.A., Nasdala, L., Norberg, N., Schaltegger, U., Schoene, B., 2008. Plešovice zircon— a new natural reference material for U–Pb and Hf isotopic microanalysis. Chemical Geology 249, 1–35.

Spencer, C.J., Cavosie, A.J., Raub, T.D., Rollinson, H., Jeon, H., Searle, M.P., Miller, J.A., McDonald, B.J., Evans, N.J., EIMF, 2017. Evidence for melting mud in Earth's mantle from extreme oxygen isotope signatures in zircon. Geology 45, 975–978.

Sun, S.S., McDonough, W.F., 1989. Chemical and isotopic systematics of oceanic basalts: implications for mantle composition and processes. In: Saunders, A.D., Norry, M.J. (Eds.), Implications for Mantle Composition and Processes. Magmatism in the Ocean Basins: Geological Society, London, Special Publication Vol. 42, pp. 313–345.

Sun, W.D., Xie, Z., Chen, J.F., Zhang, X., Chai, Z.F., Du, A.D., Zhao, J.S., Zhang, C.H., Zhou, T.F., 2003. Os–Os dating of copper and molybdenum deposits along the Middle and Lower Reaches of Yangtze River, China. Economic Geology 98, 175–180.

Sun, W.D., Ding, X., Hu, Y.H., Li, X.H., 2007. The golden transformation of the Cretaceous plate subduction in the west Pacific. Earth and Planetary Science Letters 262, 533–542.

Sylvester, P.J., 1989. Post-collisional alkaline granites. Journal of Geology 97, 261–280.

Tanaka, T., Togashi, S., Kamioka, H., Amakawa, H., Kagami, H., Hamamoto, T., Yuhara, M., Orihashi, Y., Yoneda, S., Shimizu, H., Kunimaru, T., Takahashi, K., Yanagi, T., Nakano, T., Fujimaki, H., Shinjo, R., Asahara, Y., Tanimizu, M., Dragusanu, C., 2000. JNdi-1: aneodymium isotopic reference in consistency with LaJolla neodymium. Chemical Geology 168, 279–281.

Tang, G.Q., Li, X.H., Li, Q.L., Liu, Y., Ling, X.X., Yin, Q.Z., 2015. Deciphering the physical mechanism of the topography effect for oxygen isotope measurements using a Cameca IMS-1280 SIMS. Journal of Analytical Atomic Spectrometry 30, 950–956.

Taylor, H.P., 1968. The oxygen isotope geochemistry of igneous rocks. Contributions to Mineralogy and Petrology 19, 1–71.

Trail, D., Watson, E.B., Tailby, N.D., 2012. Ce and Eu anomalies in zircon as proxies for the oxidation state of magmas. Geochimica et Cosmochimica Acta 97, 70–87.

Turner, S.P., Foden, J.D., Morrison, R.S., 1992. Derivation of some A-type magmas by fractionation of basaltic magma: an example from the Padthaway Ridge, South Australia. Lithos 28, 151–179.

Valley, J.W., 2003. Oxygen isotope in zircon. In: Hanchar, J.M., Hoskin, P.W.O. (Eds.), Reviews in Mineralogy and Geochemistry: Zircon. Mineralogical Society of America, Washington, pp. 343–380.

Valley, J.W., Kinny, P.D., Schulze, D.J., Spicuzza, M.J., 1998. Zircon megacrysts from kimberlite: oxygen isotope variability among mantle melts. Contributions to Mineralogy and Petrology 133, 1–11.

Valley, J.W., Lackey, J.S., Cavosie, A.J., Clechenko, C.C., Spicuzza, M.J., Basei, M.A.S., Bindeman, I.N., Ferreira, V.P., Sial, A.N., King, E.M., Peck, W.H., Sinha, A.K., Wei, C.S., 2005. 4.4 billion years of crustal maturation: oxygen isotope ratios of magmatic zircon. Contrib. Miner. Petrol. 150, 561–580.

Wang, F.Y., Liu, S.A., Li, S.G., He, Y.S., 2013. Contrasting zircon Hf–O isotopes and trace elements between ore-bearing and ore-barren adakitic rocks in central-easternChina: implications for genetic relation to Cu–Au mineralization. Lithos 156–159, 97–111.

Wang, F.Y., Liu, S.A., Li, S.G., Akhtar, S., He, Y.S., 2014. Zircon U–Pb ages, Hf–O isotopes and trace elements of Mesozoic high Sr/Y porphyries from Ningzhen, eastern China: constraints on their petrogenesis, tectonic implications and Cu mineralization. Lithos 200-201, 299–316.

Wang, L.X., Ma, C.Q., Zhang, C., Zhu, Y.X., Marks, M.A.W., 2018. Halogen geochemistry of I- and A-type granites from Jiuhuashan region (South China): Insights into the elevated fluorine in A-type granites. Chemical Geology 478, 164–182.

Watson, E.B., Harrison, T.M., 1983. Zircon saturation revisited: temperature and composition effects in a variety of crustal magma types. Earth and Planetary Science Letters 64, 295–304.

Webster, J.D., Tappen, C.M., Mandeville, C.W., 2009. Partitioning behavior of chlorine and fluorine in the system apatite–melt–fluid. II: felsic silicate systems at 200 MPa. Geochimica et Cosmochimica Acta 73, 559–581.

Whalen, J.B., Currie, K.L., Chappell, B.W., 1987. A-type granites: geochemical characteristics, discrimination and petrogenesis. Contributions to Mineralogy and Petrology 95, 407–419.

Wickham, S.M., Alberts, A.D., Zanvilevich, A.N., Litvinovsky, B.A., Bindeman, I.N., Schauble, E.A., 1996. A stable isotope study of anorogenic magmatism in East Central Asia. Journal of Petrology 37, 1063–1095.

Wu, F.Y., Yang, Y.H., Xie, L.W., Yang, J.H., Xu, P., 2006. Hf isotopic compositions of the standard zircons and baddeleyites used in U–Pb geochronology. Chemical Geology 234, 105–126.

Wu, F.Y., Ji, W.Q., Sun, D.H., Yang, Y.H., Li, X.H., 2012. Zircon U–Pb geochronology and Hf isotopic compositions of the Mesozoic granites in southern Anhui Province, China. Lithos 150, 6–25.

Wu, K., Ling, M.X., Sun, W.D., Guo, J., Zhang, C.C., 2017. Major transition of continental basalts in the Early Cretaceous: implications for the destruction of the North China Craton. Chemical Geology 470, 93–106.

Xie, G.Q., Mao, J.W., Li, X.W., Duan, C., Yao, L., 2011. Late Mesozoic bimodal volcanic rocks in the Jinniu basin, Middle-Lower Yangtze River Belt (YRB), East China: age, petrogenesis and tectonic implications. Lithos 127, 144–164.

Xing, F.M., 1998. Geochemistry of basic rocks from the eastern part of the Yangtze magmatic belt. Geochemica 27, 258–268 (in Chinese with English abstract).

Xing, F.M., Xu, X., 1994. Two A-type granite belts from Anhui. Acta Petrologica Sinica 10, 257–269 (in Chinese with English abstract).

Yan, J., Chen, J.F., Xu, X.S., 2008. Geochemistry of Cretaceous mafic rocks from the Lower Yangtze region, eastern China: characteristics and evolution of the lithospheric mantle. Journal of Asian Earth Sciences 33, 177–193.

Yan, J., Liu, J.M., Li, Q.Z., Xing, G.F., Liu, X.Q., Xie, J.C., Chu, X.Q., Chen, Z.H., 2015. In situ zircon Hf–O isotope analyses of late Mesozoic magmatic rocks in the Lower Yangtze River Belt, central eastern China: implications for petrogenesis and geodynamic evolution. Lithos 227, 57–76.

Yang, W., Zhang, H.F., 2012. Zircon geochronology and Hf isotopic composition of Mesozoic magmatic rocks from Chizhou, the Lower Yangtze Region: constraints on their relationship with Cu–Au mineralization. Lithos 150, 37–48.

Yang, J.H., Wu, F.Y., Chung, S.L., Wilde, S.A., Chu, M.F., 2006. A hybrid origin for theQianshan A-type granite, northeast China: geochemical and Sr–Nd–Hf isotopic evidence. Lithos 89 (1–2), 89–106.

Zhang, S., Zhang, Z.C., Ai, Y., Yuan, W.M., Ma, L.T., 2009. The petrology, mineralogy and geochemistry study of the Huangshan granite intrusion in Anhui Province. Acta Petrologica Sinica 25 (1), 25–38 (in Chinesewith English abstract).

Zhang, C., Holtz, F., Ma, C., Wolff, P.E., Li, X., 2012. Tracing the evolution and distribution of F and Cl in plutonic systems from volatile-bearing minerals: a case study from the Liujiawa pluton (Dabie orogen, China). Contributions to Mineralogy and Petrology 164, 859–879.

Zhao, Z.F., Zheng, Y.F., 2003. Calculation of oxygen isotope fractionation in magmatic rocks. Chemical Geology 193, 59–80.

Zhao, L., Guo, F., Fan, W.M., Zhang, Q.W., Wu, Y.M., Li, J.Y., Yan, W., 2016. Early Cretaceous potassic volcanic rocks in the Jiangnan Orogenic Belt, East China: crustal melting in response to subduction of the Pacific–Izanagi ridge? Chemical Geology 437, 30–43.